Solution Structure of the Dimeric Cytoplasmic Domain of Syndecan-4[†,‡]

Joon Shin,[§] Weontae Lee,*[,§] Donghan Lee,[§,||] Bon-Kyung Koo,[§] Innoc Han,[⊥] Yangmi Lim,[⊥] Anne Woods,[@] John R. Couchman,[@,#] and Eok-Soo Oh*[,⊥]

Department of Biochemistry and Protein Network Research Center, College of Science, Yonsei University, Seoul 120-740, Korea, Division of Molecular Life Sciences and Center for Cell Signaling Research, Ewha Woman's University, Seoul 120-750, Korea, and Department of Cell Biology and Cell Adhesion & Matrix Research Center, University of Alabama at Birmingham, Birmingham, Alabama 35294

Received December 4, 2000; Revised Manuscript Received April 9, 2001

ABSTRACT: The syndecans, transmembrane proteoglycans which are involved in the organization of cytoskeleton and/or actin microfilaments, have important roles as cell surface receptors during cell−cell and/or cell−matrix interactions. Since previous studies indicate that the function of the syndecan-4 cytoplasmic domain is dependent on its oligomeric status, the conformation of the syndecan-4 cytoplasmic domain itself is important in the understanding of its biological roles. Gel filtration results show that the syndecan-4 cytoplasmic domain (4L) itself forms a dimer stabilized by ionic interactions between peptides at physiological pH. Commensurately, the NMR structures demonstrate that syndecan-4L is a compact intertwined dimer with a symmetric clamp shape in the central variable V region with a root-mean-square deviation between backbone atom coordinates of 0.95 Å for residues Leu[186]−Ala[195]. The molecular surface of the 4L dimer is highly positively charged. In addition, no intersubunit NOEs in membrane proximal amino acid resides (C1 region) have been observed, demonstrating that the C1 region is mostly unstructured in the syndecan-4L dimer. Interestingly, two parallel strands of 4L form a cavity in the center of the dimeric twist similar to our previously reported 4V structure. The overall topology of the central variable region within the 4L structure is very similar to that of 4V complexed with the phosphatidylinositol 4,5-bisphosphate; however, the intersubunit interaction mode is affected by the presence of C1 and C2 regions. Therefore, we propose that although the 4V region in the full cytoplasmic domain has a tendency for strong peptide−peptide interaction, it may not be enough to overcome the repulsion of the C1 regions of syndecan-4L.

The syndecans, which are the major family of transmembrane heparan sulfate proteoglycans, appear to have a profound influence on cell behavior (*1*−*4*). All of the syndecans (four members from mammals and one each from *Drosophila* and *Caenorhabditis elegans*) share homologous regions for glycosaminoglycan (GAG) chain attachment and a putative protease cleavage site in the ectodomain proximal to the membrane. Their transmembrane and cytoplasmic domain sequences are highly conserved (*1*−*4*). This high degree of conservation of the primary structure of the cytoplasmic domains of the syndecans suggests a possible biological role for the cytoplasmic domain. Indeed, during cell−cell and/or cell−matrix interaction, syndecans have important roles as cell surface receptors (*1*−*4*), and all syndecans are known to be involved in the organization of the microfilament cytoskeleton (*1*−*8*). In particular, syndecan-4 has been of interest, since it is selectively enriched and widespread in focal adhesions (*7*).

When plated on fibronectin, normal primary fibroblasts interact with fibronectin through at least two cell surface receptors: integrin and cell surface heparan sulfate proteoglycan (*8*−*10*). The interaction with integrin transduces several signals, including tyrosine kinase activation (*11*−*13*), which are only sufficient for attachment and spreading. An additional stimulus (*1*, *8*, *14*, *15*) is needed for cytoskeletal and membrane reorganization to form stress fibers and focal adhesions, which comes from the heparin binding domain of fibronectin interacting with syndecan-4 (*14*). Thus, two signals coordinately regulate focal adhesion and stress fiber formations (*15*).

The syndecan family is known to form homologous dimers or multimers that are resistant to treatment with sodium dodecyl sulfate (SDS)[1] (*1*, *16*). Consistently, the recombinant

[†] This work was supported by the Korea Science and Engineering Foundation (KOSEF) through the Center for Cell Signaling Research at Ewha Woman's University (to E.-S.O.), by Korean Research Foundation Grant KRF-99-042-D00096 (to W.L. and E.-S.O.), and in part by the Brain Korea 21 Project. This work was also supported in part by NIH Grant GM50194 and Sankyo Co. Ltd. (J.R.C.).

[‡] The atomic coordinates for 15 simulated annealing structures, restrained energy-minimized average structures, and experimental restraints have been deposited in the Protein Data Bank (entry 1EJP).

* To whom correspondence should be addressed. W.L.: Department of Biochemistry, College of Science, Yonsei University, Seodaemoon-Gu, Shinchon-dong, Seoul 120-740, Korea; phone, 82-2-2123-2706; fax, 82-2-362-9897; e-mail, wlee@nestis.yonsei.ac.kr. E.-S.O.: Center for Cell Signaling Research, Ewha Woman's University, Daehyun-dong, Seodaemoon-Gu, Seoul 120-750, Korea; phone, 82-2-3277-3761; fax, 82-2-3277-3760; e-mail, OhES@mm.ewha.ac.kr.

[§] Yonsei University.

[||] Present address: Institute for Molecular Biology and Biophysics, ETH, Zurich, Switzerland.

[⊥] Ewha Woman's University.

[@] University of Alabama at Birmingham.

[#] Present address: Biomedical Sciences Division, Imperial College School of Medicine, London SW7 2AZ, U.K.

10.1021/bi002750r CCC: $20.00
Published on Web 06/29/2001

syndecan-3 core protein forms stable, noncovalent multimer complexes through the transmembrane domain and the ectodomain flanking region (*17*), and recombinant proteins of both syndecan-2 and -4 core proteins form SDS-resistant oligomers even in the absence of the whole cytoplasmic domain (*18*, *19*). Thus, the cytoplasmic domain of syndecan-4 is not essential for basal oligomerization. Biochemical studies with synthetic peptides show divergence in oligomerization; the whole cytoplasmic domain of syndecan-1 and -2 may be mostly monomer. In contrast, the synthetic peptide corresponding to the whole cytoplasmic domain of syndecan-4 (4L) forms a dimer (*19*). Furthermore, synthetic peptides from the central variable region of the syndecan-4 cytoplasmic domain (4V) exhibit a much higher multimeric status than 4L. Interestingly, this difference between 4L and 4V is strongly correlated with the ability of syndecan-4 peptides to regulate protein kinase Cα (PKCα) activity in vitro (*18*). In the presence of phosphatidylinositol 4,5-bisphosphate (PIP_2), 4L becomes a high-order oligomer and able to upregulate PKCα activity, confirming a critical role for multimerization of the syndecan-4 cytoplasmic domain in the regulation of PKCα activity (*18*, *20*). Recently, it has been found that serine phosphorylation (Ser^{183}) of the syndecan-4 cytoplasmic tail in vivo (*21*, *22*) reduced its ability to activate PKCα by preventing PIP_2-dependent oligomerization of the syndecan-4 cytoplasmic domain, not by affecting its ability to bind PKCα (*22*). This strongly suggests that, in vivo, the multimerization status of the syndecan-4 cytoplasmic domain is very critical for the function of syndecan-4.

The syndecan-4 cytoplasmic domain itself may have two different tendencies for oligomerization (dimers and higher-order oligomers), and this may be important for its cytoplasmic domain in regulating PKC activity during focal adhesion formation. Thus, it is very important to determine the three-dimensional structure of the whole cytoplasmic domain. Previously, we have reported that the 4V peptide dimerized in a parallel twisted clamp structure and that this is stabilized by PIP_2 (*23*). However, since the complete syndecan-4 cytoplasmsmic domain consists of N- and C-terminal constant regions (C1 and C2) flanking the variable region (V), the function of amino acid residues in the 4V region may be affected by the constant regions. In particular, the membrane-proximal region C1, which is highly basic, could affect protein−protein interactions, thereby changing the three-dimensional structure of the whole cytoplasmic domain. Therefore, the solution structure of the synthetic full-length syndecan-4 cytoplasmic domain (4L) would provide invaluable information for syndecan functions. Here, we report the NMR structural results of syndecan-4L determined by two-dimensional NMR spectroscopy and simulated annealing calculations.

EXPERIMENTAL PROCEDURES

Sample Preparations. The 4L cytoplasmic domain (RMKKKDEGSYDLGKKPIYKKAPTNEFYA) corresponding to residues 175−202 of the rat sequence was synthesized using an improved version of the solid-phase method (Peptron Inc., Taejon, Korea). The sequences of the human, rat, and chicken syndecan-4L domains are identical. We also synthesized the 4Lcys peptide containing the additional cysteine residue added to the N-terminus of the 4L peptide. The peptide was purified by reverse-phase liquid chromatography using a Nova-Pak C18 column on a Waters Delta Prep 4000 system. Purification was achieved by equilibrating the column with 0.1% TFA in water and developing with a linear gradient of acetonitrile. Peptide sequences were confirmed by both high-pressure liquid chromatography (HPLC) and mass spectrometry. The peptide samples for NMR measurements were prepared by dissolving them in a 90% H_2O/10% D_2O or 99.9% D_2O solution at pH 7.4 with 50 mM sodium phosphate buffer. The final peptide concentration was adjusted to 2−4 mM.

Size Exclusion Chromatography. The syndecan-4L peptides (2 mg/mL, 10 μL) were loaded onto Sephadex G-50 (0.6 cm × 30 cm) gel filtration columns pre-equilibrated with each buffer: 20 mM Na_2PO_4 (pH 4.0), 50 mM HEPES (pH 7.2), and 20 mM glycine (pH 10.0) with 150 mM NaCl. Peptides were eluted with the same buffer at a flow rate of 6 mL/h at room temperature and detected by measuring the absorbance at 280 nm. For the oxidation of 4Lcys, the peptide was preincubated with different concentrations of H_2O_2 as indicated. Oxidized 4Lcys was subjected to 20% SDS−PAGE in the absence or presence of 1 mM DTT. Some samples were loaded onto columns pre-equilibrated under the same conditions. The column was calibrated using carbonic anhydrase (29.0 kDa), equine myoglobin (17.0 kDa), lysozyme (14.3 kDa), aprotinine (6.5 kDa), and vitamin B_{12} (1.3 kDa).

NMR Spectroscopy. All NMR experiments were performed on a Bruker DRX500 spectrometer in quadrature detection mode equipped with a triple-resonance probe head with triple-axis gradient coils. All data were collected at both 5 and 25 °C, and the strong solvent resonance was suppressed by a water-gated pulse sequence combined with pulsed-field-gradient (PFG) pulses. Mixing times of 50−400 ms were used in collecting NOE spectra for syndecan-4L. Total correlation spectroscopy (TOCSY) data were also recorded in both H_2O and D_2O solutions with a mixing time of 78 ms using MLEV17 spin lock pulses (*24*). Double-quantum-filtered (DQF) COSY (*25*) spectra were collected in an H_2O solution to obtain vicinal coupling constants. All data were recorded in the phase sensitive mode using the time-proportional phase incrementation (TPPI) method (*26*) with 2048 data points in the t_2 domain and 256 in the t_1 domain. Two-dimensional NOESY (*27*) experiments were also performed to identify slow-exchanging amide hydrogens on a freshly prepared D_2O solution after lyophilization of an H_2O sample.

All NMR data were processed using Bruker XWIN NMR (Bruker Instruments) software on an SGI Indigo^2 workstation and analyzed using Sparky 3.60 software. Prior to Fourier transformation in the t_1 dimension, the first row was half-weighted to suppress t_1 ridges (*28*). The DQF-COSY data were processed to 8192 × 1024 data matrixes to obtain a maximum digital resolution for coupling constant measurements. The proton chemical shifts were referenced to internal sodium 4,4-dimethyl-4-silapentane 1-sulfonate (DSS).

[1] Abbreviations: V, variable; C, constant; PIP2, phosphatidylinositol 4,5-bisphosphate; PKC, protein kinase C; SDS, sodium dodecyl sulfate; NOESY, nuclear Overhauser effect spectroscopy; NOE, nuclear Overhauser effect; TOCSY, total correlation spectroscopy; DQF, double-quantum-filtered; COSY, correlation spectroscopy; SA, simulated annealing.

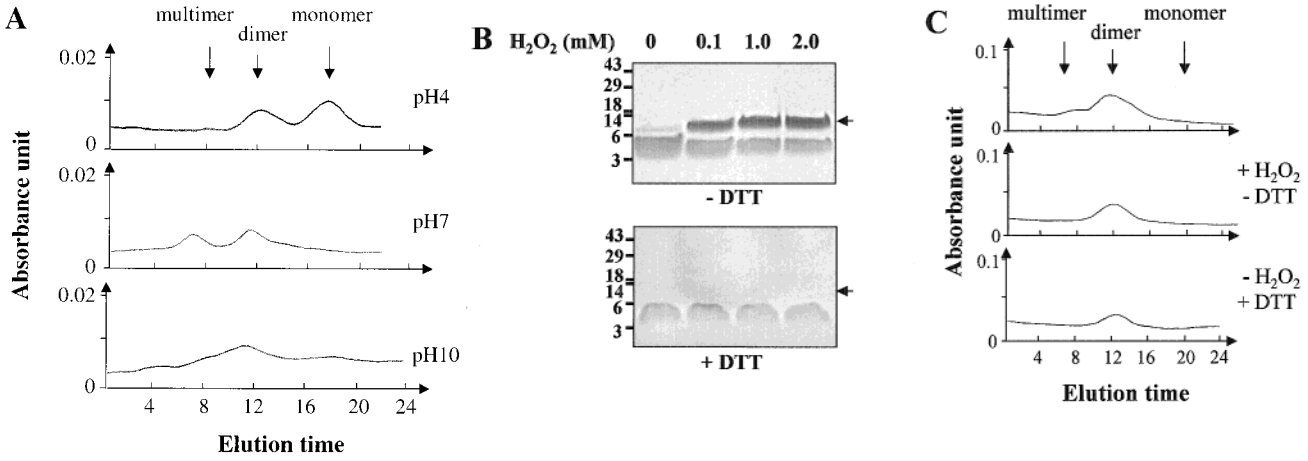

FIGURE 1: (A) Sephadex G-50 gel filtration chromatography of syndecan-4L. Gel filtration was performed at different pHs as indicated. The approximate elution positions for the monomeric, dimeric, and multimeric forms are shown on the basis of the elution of protein standards. (B) Dimer formation of 4Lcys on SDS−PAGE after oxidation. 4Lcys was preincubated with H_2O_2 and then run on 20% SDS−PAGE either in the absence (upper panel) or in the presence of DTT (lower panel). Arrows show dimeric 4Lcys. (C) Sephadex G-50 gel filtration chromatography of the 4Lcys peptide.

Structural Restraints and Modeling Calculations. Structure calculations were performed for syndecan-4L using XPLOR 3.851 (Biosym/Molecular Simulations, Inc.) on an SGI Indigo^2 workstation using the topology and parameter files of topallhdg.pro and parallhdg.pro. NMR structures were calculated by the hybrid distance geometry and simulated annealing (SA) calculations (*29*−*32*). For generation of the symmetric dimer, the method developed by Nilges (*29*) was successfully employed with minor modifications as described by Lee et al. (*33*). Symmetric dimers were generated by duplications of the random coordinates, and the combined use of XPLOR NCS and symmetry pseudo-NOE terms served to satisfy monomer symmetry as described by Nilges (*29*). The symmetry restraints were tested on the NOE data set at the intermediate modeling stage in the refinement (*33*). Two different classes of NOE constraints were also used for structure generation, which are ambiguous NOEs and intersubunit NOEs for dimer structure. The potential energy function consisted of covalent, repulsion, NOE, and torsion angle terms. The target function forms of NOE and torsion angles are the same as those used by Driscoll et al. (*34*). A total of 294 distance restraints and 16 torsion angles were used for the calculations. All NOEs were classified and converted to distance constraints as strong (1.8−2.7 Å), medium (1.8−3.3 Å), and weak (1.8−5.0 Å) on the basis of their intensities derived from the NOESY spectrum. Corrections for pseudoatom representations were used for nonstereospecifically assigned methylene, methyl group, and tyrosine ring protons (*26*). Dihedral angle restraints were derived from measured $^3J_{HN-H\alpha}$ coupling constants in DQF-COSY spectra in an H_2O solution (*35*, *36*). The final structure of the syndecan-4L dimer was analyzed and displayed with Insight II (Biosym/Molecular Simulations Inc.).

RESULTS AND DISCUSSION

Syndecan-4L Forms a Dimer. Previous biochemical studies indicated that the 4L peptide could be dimeric, since gel filtration showed a molecular weight ~2 times higher than the predicted value (*19*). However, the fact that the 4L peptide may run unusually higher has been questioned, because it is not a globular protein. To exclude this possibility, we attemped to resolve the dimer of 4L into monomers by changing the experimental conditions. Since protein−protein interactions can be stabilized through the ionic interaction, we incubated the 4L peptide at different pH values, and then performed Sephadex G-50 gel filtration column chromatography (Figure 1A). At pH 7.0, as previously shown, most of the 4L peptide eluted at approximately 2 times the predicted molecular weight, demonstrating its dimeric status. We could also detect a fraction of the multimeric unit, although it was variable. At pH 4, however, we could detect a small population of a dimeric conformation, but most of 4L eluted in a monomeric position, strongly suggesting that at physiological pH, syndecan-4L forms a dimer stabilized by ionic interaction between peptides. At pH 10, the pattern was similar to that at pH 7.0 except for broadening peaks. Therefore, we concluded that syndecan-4L prefers a dimer conformation under physiological conditions. We further confirmed the formation of the 4L dimer using the 4Lcys peptide containing the additional cysteine at the N-terminus of 4L (Figure 1B,C). We preincubated the 4Lcys peptide with varying concentrations of H_2O_2 to induce disulfide bond formation, and then performed 20% SDS−PAGE either in the presence or in the absence of reducing agent DTT. In contrast to gel filtration column chromatography, SDS denatured 4Lcys into a monomer. However, H_2O_2-oxidized 4Lcys formed disulfide bonds, and in the absence of DTT, dimeric 4Lcys was observed (Figure 1B, upper panel). This dimeric 4Lcys was reduced to a monomer by the addition of DTT (Figure 1B, lower panel). Under the same conditions, gel filtration chromatography of the 4Lcys peptide showed dimer formation (Figure 1C). This dimeric formation of 4Lcys was independent of either H_2O_2 or DTT. All these results strongly support the fact that at neutral pH, syndecan-4L forms a stable dimer.

A dimeric form of the cytoplasmic domain was also confirmed with the recombinant syndecan-4 cytoplasmic domain peptide (Figure 2). The purified GST−syndecan-4 fusion protein containing only the cytoplasmic domain (GST−4Cyto) was incubated with thrombin to remove GST. Then, the purified recombinant syndecan-4 cytoplasmic domain (4Cyto) was subjected to SDS−PAGE. Like the 4L

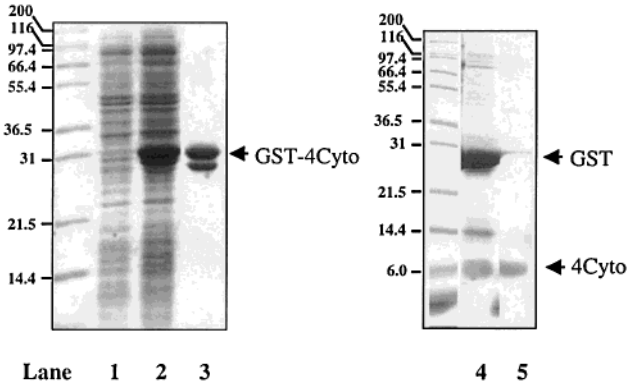

FIGURE 2: Formation of a dimer of the recombinant syndecan-4 cytoplasmic domain on SDS−PAGE. The GST−syndecan-4 fusion protein containing only the cytoplasmic domain (GST−4Cyto) was expressed (lane 2) and purified using glutathione−agarose beads (lane 3). After GST−4Cyto was incubated with thrombin to cleave GST (lane 4), GST was removed using glutathione−agarose beads (lane 5). The recombinant syndecan-4 cytoplasmic domain (4Cyto) is marked.

FIGURE 3: Summary of the sequential and medium-range NOE connectivities identified in syndecan-4L at 25 °C and pH 7.4. The mixing times of 50−400 ms were used, and observed NOE intensities were classified by the thickness of the lines.

peptide, 4Cyto migrated on SDS−PAGE as a single population with an apparent M_r of ~6.0 kDa, confirming dimeric formation of the cytoplasmic domain. Consistent with previous results using either the wild-type syndecan-4 core protein or the 4L peptide, recombinant 4Cyto demonstrated PKCα activity in the presence of PIP_2 (data not shown). Therefore, the oligomeric status of the syndecan-4 cytopalsmic domain is critical to regulation of syndecan-4 activity.

Resonance Assignments and Secondary Structures. There are two glycine, three tyrosine, and two alanine residues in the syndecan-4L sequence. Glycines were easily identified by their distinctive fingerprint in the DQF-COSY spectra in an H_2O solution, and the two alanine residues were also identified from connectivities in TOCSY spectra by their characteristic methyl resonance. The three tyrosine residues were easily assigned by combined use of TOCSY and NOESY spectra. The single serine residue was also assigned from the TOCSY spectrum. These preliminary resonance assignments served as starting points for the sequence-specific assignment procedure (*37*). Sequential resonance assignments were made from two-dimensional TOCSY and NOESY spectra in a 90% H_2O/10% D_2O solution. The identification of side chain resonance was completed with TOCSY connectivities. All these sequential and medium-range NOE connectivities for syndecan-4L are summarized in Figure 3**.** Residues 175−180 are unstructured, and no standard secondary structural elements are observed. All NOEs (Figure 3) were observed at mixing times of 50−400 ms. Figure 4 displays a two-dimensional NOESY proton spectrum with a mixing time of 200 ms at 25 °C, labeled with intramolecular NOEs as well as intermolecular NOEs. A schematic diagram of both intermolecular NOEs (between peptides) is presented in Figure 5, which also shows the sequences corresponding to the C1, V, and C2 regions of the syndecan-4 cytoplasmic domain.

Table 1: Structural Statistics for the Final Simulated Annealing (SA) Structures of the Syndecan-4 Cytoplasmic Domain

	$\langle SA \rangle_k$	$\langle \overline{SA} \rangle_{kr}$
rms deviations from experimental distance restraints (Å)		
all (294)	0.026	0.02367
intramonomer (246)	0.02807	0.03825
intermonomer (48)	0.00262	0.01272
energies (kcal/mol)		
E_{total}	89.48	96.81
E_{NOE} (all)	10.015	18.34
E_{tor}	66.285	63.1
E_{L-J}	−42.878	−50.99
E_{NCS}	0.0012	0.0015
deviations from idealized covalent geometry		
bonds (Å)	0.0015	0.0016
angles (deg)	0.4992	0.4871
impropers (deg)	0.3480	0.3831
rms deviation of structural segment for $\langle SA \rangle_k$ (Leu^{186}−Ala^{195}) (Å)		
backbone	0.95 ± 0.32	
heavy atoms	1.66 ± 0.38	

Solution Structure of the 4L Dimer. This report and previous reports (*19*, *38*) have shown that the syndecan-4L peptide itself forms a dimer, by chromatograpahic analysis. The solution structures of syndecan-4L calculated using the experimental constraints demonstrated symmetric dimers with two twisted parallel strands. A total of 90 starting substructures were calculated in the initial simulated annealing stage. After two cycles of the simulated annealing protocol, 60 structures which showed no constraint violations greater than 0.5 Å for distances and 5° for torsional angles were identified. Among 60 structures, the 15 lowest-energy structures ($\langle SA \rangle_k$) were selected for structural analysis. The structures are well defined with a root-mean-square deviation between backbone atom coordinates of 0.95 Å for residues Leu^{186}−Ala^{195} (Figure 6A). The average structure was generated from the geometrical average from 15 structure coordinates and was subjected to restrained energy minimization to correct bond length and angle distortions. This average structure exhibited an rms deviation of 0.63 Å for backbone atoms for the structurally well-defined region with respect to 15 $\langle SA \rangle_k$ structures (Figure 6B). A best-fit superposition of all final structures and the backbone conformation for the average REM structure ($\langle \overline{SA} \rangle_{kr}$) for syndecan-4L are shown in Figure 6A. Energies and structural statistics for 15 $\langle SA \rangle_k$ and $\langle SA \rangle_{kr}$ structures are listed in Table 1. The atomic average rms deviations of the final structures with respect to the average REM structure are shown in Figure 7. The Ramachandran plot indicated that the φ and ϕ values of all 15 final NMR structures were distributed properly in an energetically acceptable region (data not shown) (*39*). The overall conformation is a compact intertwined dimer having an unusual symmetric clamp shape. In addition, the molecular surface is highly positively charged

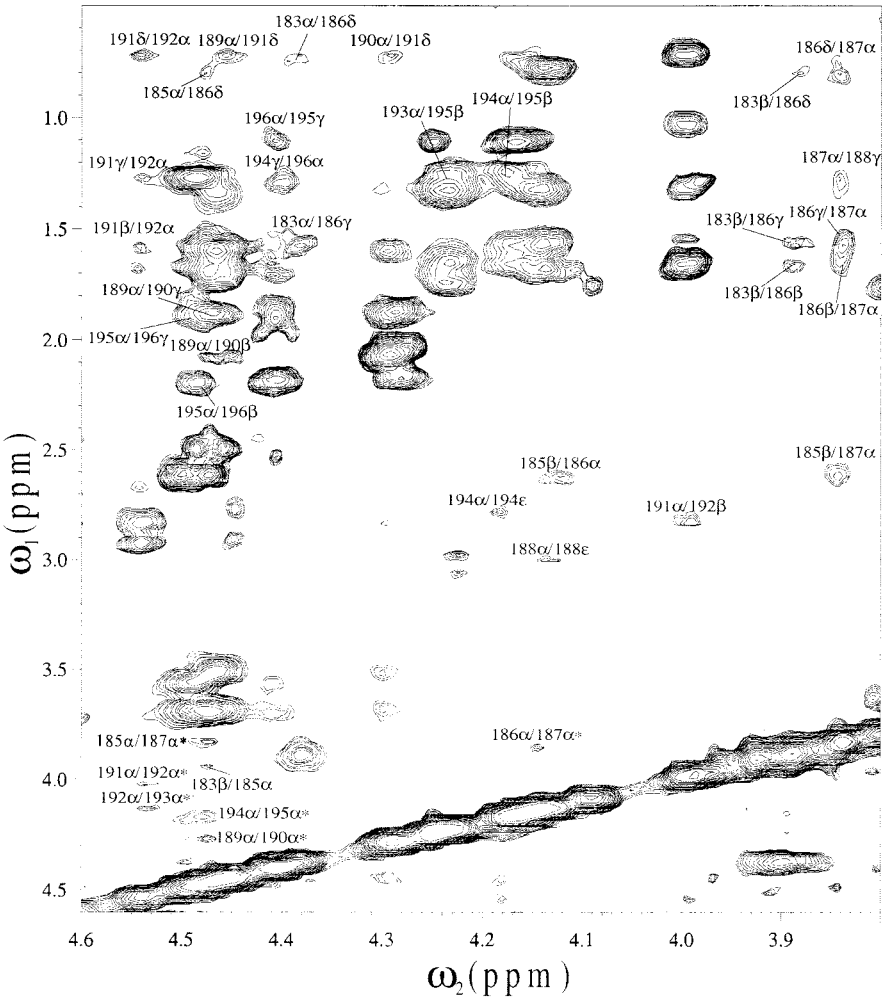

FIGURE 4: Two-dimensional NOESY proton spectrum (500 MHz) of syndecan-4L with mixing time of 200 ms in a D_2O solution at 25 °C. The spectrum demonstrates intramolecular NOEs as well as intermolecular NOEs marked with asterisks.

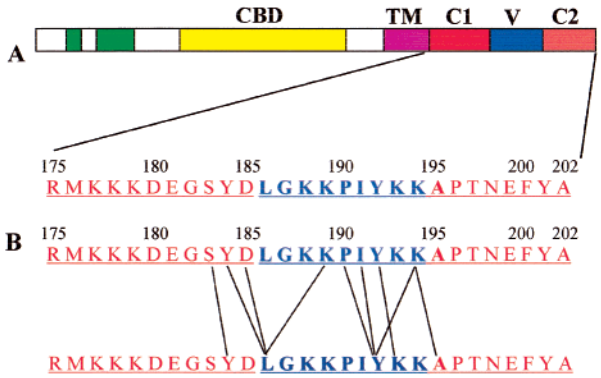

FIGURE 5: Schematic diagram of the syndecan-4 protein and intermomecular NOE interactions observed for syndecan-4L. (A) Functional domains of the syndecan-4 protein are represented as boxes. (B) Observed intermolecular NOEs between monomers in syndecan-4L are represented as lines.

and two parallel strands form a cavity in the center of the dimeric twist similar to our previously reported 4V structure as shown in Figure 8 (*23*). Both the C1 and C2 terminal regions exhibited extensive flexibility. In general, even though the overall topology of the 4V region within the 4L structure is very similar to that of the 4V−PIP_2 complex, the intersubunit interaction mode is affected by the C1 and C2 domains (Figure 6).

Previously, we have also shown the importance of multimerization of the syndecan-4 core protein, since only oligomeric forms of both recombinant and cytoplasmic domain peptides can regulate PKCα activity (*18*, *19*). Thus, both oligomerization and structural reorganization of syndecan-4 in space are important for the syndecan-4 cytoplasmic domain regulating both the distribution and activity of PKC. In this report, we have presented the solution structure of syndecan-4L. Major intersubunit interactions were detected in the central variable region, consistent with our early report for the function of the 4V peptide (*23*). Recently, it has also been reported that the central variable region in the syndecan cytoplasmic domain is involved in functional regulation. These data might explain how syndecan-4, but not syndecan-2, could regulate focal adhesion and stress fiber formation in fibroblasts, although all syndecans seemed to be involved in cytoskeleton organization during cell−matrix interaction (*1*, *6*, *14*, *15*). It will be very interesting to determine how the unique V regions in each syndecan affect the three-dimensional structure of syndecan cytoplasmic domains. In addition, it will be informative to see how the PDZ proteins such as syntenin, interacting at the C-terminal FYA motif (*40*), or other syndecan binding proteins regulate structural changes of the cytoplasmic domain (*1*, *15*, *18*, *22*, *41*). This is because intersubunit interactions of the C1 and C2 regions participate in dimer formation, even though the variable

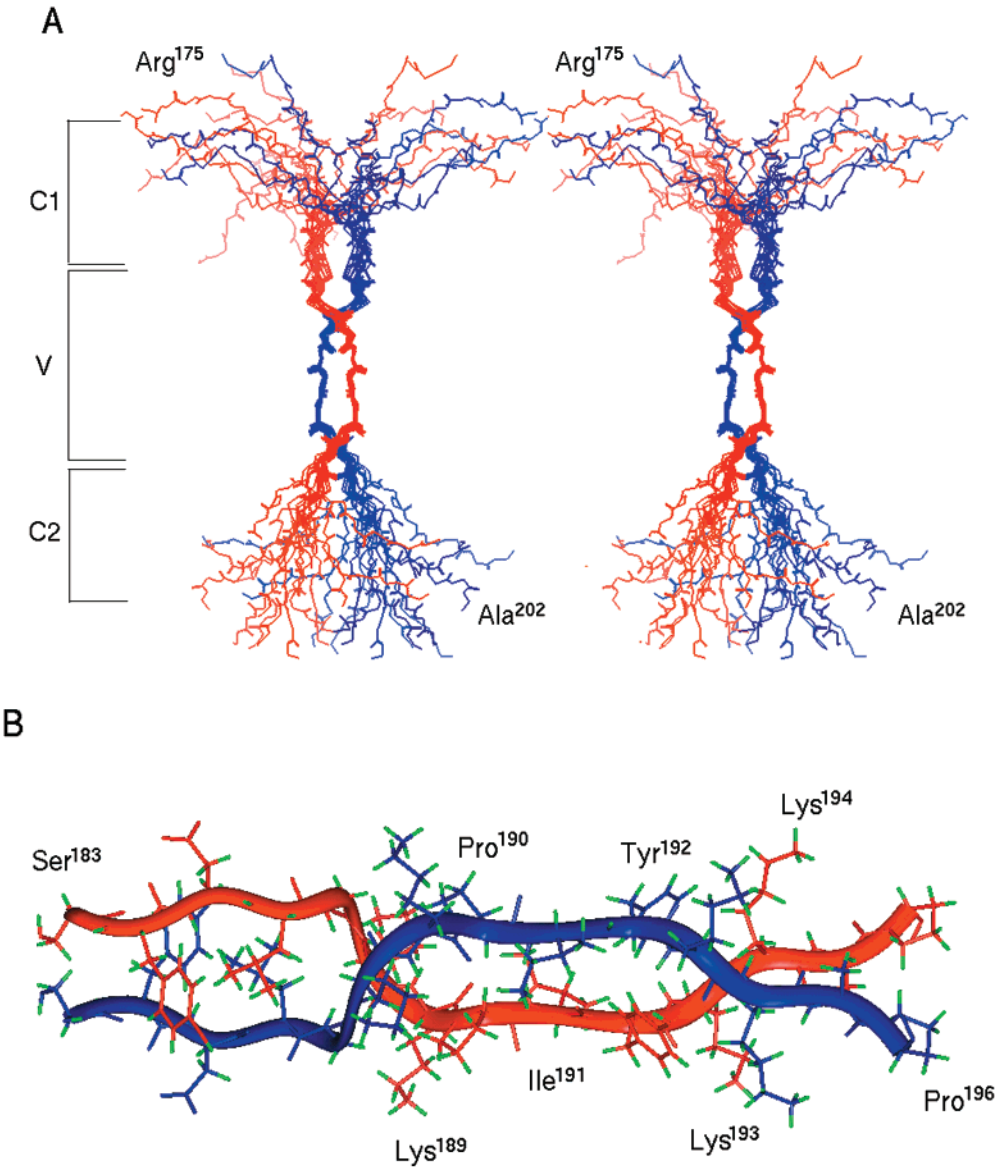

FIGURE 6: Solution structures of syndecan-4L. (A) Dimeric structures of syndecan-4L generated from NMR constraints. A stereoview of the backbone superposition of the energy-minimized average structure ($\langle\overline{SA}\rangle_{kr}$) over the family of 15 final simulated annealing structures ($\langle SA\rangle_k$) is displayed with subunits A (red) and B (blue). (B) A stick model of the energy-minimized average structure displaying all atoms. Backbone conformations of subunits are also drawn as red and blue ribbons, respectively.

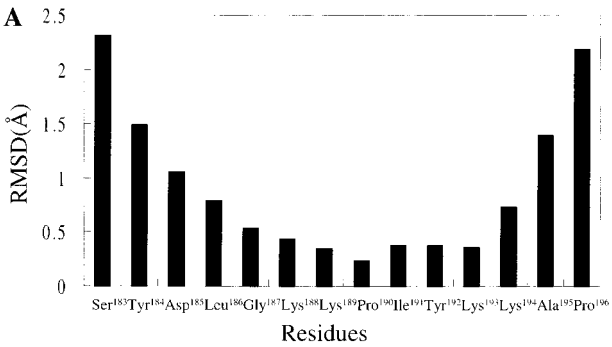

FIGURE 7: Distribution of the backbone average atomic rms deviations for residues Ser^{183}−Ala^{195} with respect to the average structure of syndecan-4L in the final simulated annealing structures.

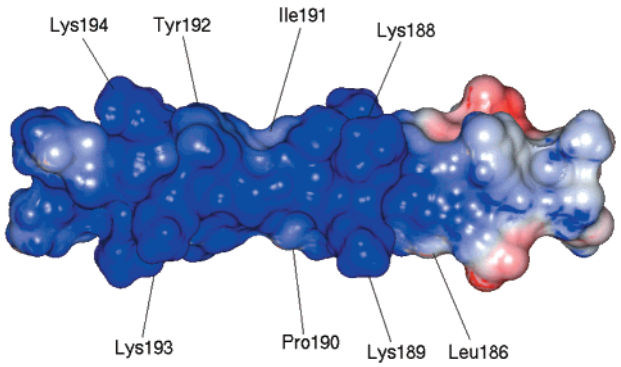

FIGURE 8: Electrostatic potential surface of syndecan-4L. The negative electrostatic potential is represented in red, the positive in blue, and the neutral in white. The potential surface was calculated using the Delphi program (Biosym/Molecular Simulations Inc.).

region is mainly responsible for oligomerization of syndecan-4. Consistent with these data, recent biochemical studies have shown that phosphorylation of Ser^{183} destabilized the oligomerization of the syndecan-4 cytoplasmic domain, with the concomitant loss of PKC activation (*21*). In this report, we have shown intersubunit NOEs between Ser^{183} and Tyr^{184}, which contribute to stability for the dimeric conformation.

Therefore, it is consistent that phosphorylation of Ser^{183} destabilizes protein−protein interactions required for oligomerization. In our previous biochemical data (*7*), we failed to detect a higher oligomeric form of the 4V peptide under the conditions used for NMR. This may be explained by the flexible nature of the small peptides due to temperature effects. Therefore, the flexibility was removed by addition of PIP_2, resulting in a stable 4V−PIP_2 complex in our previous report (*23*).

It is possible that the highly basic C1 region of syndecan-4 could interrupt intersubunit interactions between 4L peptides. Consistently, no intersubunit NOEs in membrane proximal amino acid resides (C1 region) have been observed (Figure 5). As a result, our NMR structure clearly showed that the C1 region is mostly unstructured in the syndecan-4L dimer (Figure 6A). Therefore, although the 4V region in the full cytoplasmic domain has a tendency for strong peptide−peptide interaction, it may not be enough to overcome the repulsion of the C1 regions. For the syndecan-4 cytoplasmic domain to be oligomerized in vivo, highly basic charges in the C1 region may have to be at least neutralized, perhaps through interactions with acidic phospholipids in plasma membrane, or other cytosolic proteins (Figure 8). We propose here that the 4L cytoplasmic domain itself can form a symmetric dimer through monomer−monomer interaction. However, the structural role of the C1, which may be constrained in vivo by the presence of the membrane-spanning domain and the C2 region related to PKC binding, is still not clear. We have already shown that PIP_2 induces higher-order oligomerization of the cytoplasmic domain and described the interaction between PIP_2 and the 4V region (*19*, *23*). NMR analysis demonstrates that in the presence of PIP_2, the 4V region itself interacts more strongly with the other subunit, forming a stable dimer. Even though the variable region is mainly responsible for oligomerization of syndecan-4, intersubunit interactions in the C1 and C2 regions also play an important role for dimer structure. Whether this impacts the potential interaction of the C2 domain with PDZ proteins (*40*) remains to be established. These findings suggest that not only the variable region but also the C2 region could play an important role in syndecan oligomerization processes.

Our working hypothesis is that the cytoplasmic domains of syndecan-4 are localized in a juxtamembrane complex through the V region binding to inositol phospholipid. Tertiary structural studies, including techniques for isotopically labeling of the cytoplasmic domain together with PKCα and PIP_2, will provide insights into this signaling complex and are currently in progress.

ACKNOWLEDGMENT

We thank professor T. L. James for providing the Sparky program.

REFERENCES

1. Bernfield, M., Gotte, M., Park, P. W., Reizes, O., Fitzgerald, M. L., Lincecum, J., and Zako, M. (1999) *Annu. Rev. Biochem. 68*, 729−777.
2. Rapraeger, A. C., and Ott, V. L. (1998) *Curr. Opin. Cell Biol. 10*, 620−628.
3. Couchman, J. R., and Woods, A. (1998) *Trends Cell Biol. 8*, 189−192.
4. Carey, D. J. (1997) *Biochem. J. 327*, 1−16.
5. Carey, D. J., Stahl, R. C., Cizmeci-Smith, G., and Asundi, V. K. (1994) *J. Cell Biol. 124*, 161−170.
6. Longley, R. L., Woods, A., Fleetwood, A., Cowling, G. J., Gallagher, J. T., and Couchman, J. R. (1999) *J. Cell Sci. 112*, 3421−3431.
7. Woods, A., and Couchman, J. R. (1994) *Mol. Biol. Cell 5*, 183−192.
8. Woods, A., McCarthy, J. B., Furcht, L. T., and Couchman, J. R. (1993) *Mol. Biol. Cell 4*, 605−613.
9. Ruoslahti, E. (1996) *Annu. Rev. Cell Dev. Biol. 12*, 697−715.
10. Bloom, L., Ingham, K. C., and Hynes, R. O. (1999) *Mol. Biol. Cell 10*, 1521−1536.
11. Miyamoto, S., Teramoto, H., Coso, O. A., Gutkind, J. S., Burbelo, P. D., Akiyama, S. K., and Yamada, K. M. (1995) *J. Cell Biol. 131*, 791−805.
12. Clark, E. A., and Brugge, J. S. (1995) *Science 268*, 233−239.
13. Burridge, K., and Chrzanowska-Wodnicka, M. (1996) *Annu. Rev. Cell Dev. Biol. 12*, 463−518.
14. Saoncella, S., Echtermeyer, F., Denhez, F., Nowlen, J. K., Mosher, D. F., Robinson, S. D., Hynes, R. O., and Goetinck, P. F. (1999) *Proc. Natl. Acad. Sci. U.S.A. 96*, 2805−2810.
15. Couchman, J. R., and Woods, A. (1999) *J. Cell Sci. 112*, 3415−3420.
16. Pierce, A., Lyon, M., Hampson, I. N., Cowling, G. J., and Gallagher, J. (1992) *J. Biol. Chem. 267*, 3894−3900.
17. Asundi, V. K., and Carey, D. J. (1995) *J. Biol. Chem. 270*, 26404−26410.
18. Oh, E. S., Woods, A., and Couchman, J. R. (1997) *J. Biol. Chem. 272*, 8133−8136.
19. Oh, E. S., Woods, A., and Couchman, J. R. (1997) *J. Biol. Chem. 272*, 11805−11811.
20. Oh, E. S., Woods, A., Lim, S. T., Theibert, A., and Couchman, J. R. (1998) *J. Biol. Chem. 273*, 10624−10629.
21. Horowitz, A., and Simons, M. (1998) *J. Biol. Chem. 273*, 10914−10918.
22. Horowitz, A., and Simons, M. (1998) *J. Biol. Chem. 273*, 25548−25551.
23. Lee, D., Oh, E. S., Woods, A., Couchman, J. R., and Lee, W. (1998) *J. Biol. Chem. 273*, 13022−13029.
24. Bax, A., and Davis, D. G. (1985) *J. Magn. Reson. 65*, 355−360.
25. Rance, M., Soerensen, O. W., Bodehausen, G., Wagner, G., Ernst, R. R., and Wuthrich, K. (1983) *Biochem. Biophys. Res. Commun. 117*, 479−485.
26. Wuthrich, K., Billeter, M., and Braun, W. (1983) *J. Mol. Biol. 169*, 949−961.
27. Jeener, J., Meier, B. H., Bachman, P., and Ernst, R. R. (1979) *J. Chem. Phys. 71*, 4546−4553.
28. Otting, G., Widmer, H., Wagner, G., and Wuthrich, K. (1986) *J. Magn. Reson. 66*, 187−193.
29. Nilges, M., Clore, G. M., and Gronenborn, A. M. (1988) *FEBS Lett. 229*, 317−324.
30. Nilges, M., Clore, G. M., and Gronenborn, A. M. (1988) *FEBS Lett. 239*, 129−136.
31. Nilges, M., Gronenborn, A. M., Brunger, A. T., and Clore, G. M. (1988) *Protein Eng. 2*, 27−38.
32. Nilges, M. (1993) *Proteins 17*, 297−309.
33. Lee, W., Harvey, T. S., Yin, Y., Yau, P., Litchfield, D., and Arrowsmith, C. H. (1994) *Nat. Struct. Biol. 1*, 877−890.
34. Driscoll, P. C., Gronenborn, A. M., Beress, L., and Clore, G. M. (1989) *Biochemistry 28*, 2188−2198.
35. Clore, G. M., Gronenborn, A. M., Nilges, M., and Ryan, C. A. (1987) *Biochemistry 26*, 8012−8023.
36. Wagner, G., Braun, W., Havel, T. F., Schaumann, T., Go, N., and Wuthrich, K. (1987) *J. Mol. Biol. 196*, 611−639.

37. Wuthrich, K. (1986) *NMR of proteins and nucleic acids*, Wiley, New York.
38. Horowitz, A., Murakami, M., Gao, Y., and Simons, M. (1999) *Biochemistry 38*, 15871−15877.
39. Morris, A. L., MacArthur, M. W., Hutchison, E. G., and Thornton, J. M. (1992) *Proteins 12*, 345−364.
40. Zimmermann, P., and David, G. (1999) *FASEB J. 13*, S91−S100.
41. Baciu, P. C., Saoncella, S., Lee, S. H., Denhez, F., Leuthardt, D., and Goetinck, P.F. (2000) *J. Cell Sci. 113*, 315−324.

BI002750R